IEEE Journal of Microwaves

Received 9 February 2023; revised 22 April 2023; accepted 18 May 2023. Date of publication 2 June 2023; date of current version 7 July 2023.

Digital Object Identifier 10.1109/JMW.2023.3279014

Improving the Precision of On-Wafer W-Band Scalar Load-Pull Measurements

NICHOLAS C. MILLER [1] (Senior Member, IEEE), MICHAEL ELLIOTT [2], EYTHAN LAM [3] (Member, IEEE), RYAN GILBERT [2] (Member, IEEE), JANSEN UYEDA [4], AND ROBERT L. COFFIE [4] (Senior Member, IEEE)

(Regular Paper)

[1]Air Force Research Laboratory Sensors Directorate, Wright-Patterson AFB, OH 45433 USA
[2]KBR, Wright-Patterson AFB, OH 45433 USA
[3]University of California, Santa Barbara, Santa Barbara, CA 93106 USA
[4]Northrop Grumman Corporation, Redondo Beach, CA 90278-1001 USA

CORRESPONDING AUTHOR: Nicholas C. Miller (e-mail: nicholas.miller.58@us.af.mil).

This work was supported by the Air Force Research Laboratory under Grant FA807518D0015.

ABSTRACT This article presents an empirical investigation of calibration effects on load-pull measurements collected on wafer and at W-band frequencies. An analysis of scattering parameter (S-parameter) measurements provides insight into how small-signal metrics germane to load pull are affected by choice of the calibration technique. It is found that off-wafer line-reflect-reflect-match (LRRM) calibrated measurements of the same transistor with different probes exhibit drastically different maximum small-signal gains compared to equivalent on-wafer multiline thru-reflect-line (mTRL) calibrated measurements. Load-pull measurements are heavily influenced by choice of calibration algorithm, and LRRM calibrated large-signal measurements collected with different waveguide probes yield variations in large-signal gain of over 2 dB and variations in peak PAE of over 24 percentage points. The equivalent on-wafer mTRL calibrated load-pull measurements collected with different waveguide probes are consistent to within 0.1 dB for large-signal gain and 1 percentage point for peak PAE. This work provides quantitative evidence that on-wafer mTRL calibration with well-designed calibration structures is preferred for large-signal measurements collected at millimeter-wave frequencies. If utilization of on-wafer mTRL calibration is not possible, this work suggests using similar measurement setups, i.e., waveguide probes, calibration standards, etc., for evaluating on-wafer unmatched transistors in a consistent manner.

INDEX TERMS Calibration, load-pull, LRRM, measurements, scattering-parameters, TRL, W-band.

I. INTRODUCTION

On-wafer large-signal measurements at millimeter-wave (mm-wave) frequencies have received considerable attention in the past few years due to interest in microelectronics applications above Ka-band frequencies. Load-pull measurements are important for device characterization, model extraction and validation, and characterization and validation of the resulting mm-wave monolithic microwave integrated circuits. However, at mm-wave frequencies, measurement systems become rare. A W-band passive load-pull system was reported in [1] for evaluating the large-signal performance of nitrogen-polar gallium nitride (GaN) high electron mobility transistors (HEMTs). An active load-pull system designed for W-band frequency operation was developed by Teppati et al. in [2]. In [3], a commercial W-band vector-receiver hybrid active load-pull system was presented. A scalar W-band load-pull system was employed in [4] for nonlinear circuit model validation.

The most critical aspect of on-wafer measurements is the calibration of the system. Calibration establishes reference planes of the corrected measurements at a desired location and removes systematic errors from the instrument hardware [5]. There exists a wide range of calibration algorithms and techniques for on-wafer scattering-parameter (S-Parameter) measurements. The traditional short-open-load-thru (SOLT) calibration technique is ubiquitous throughout the on-wafer

radio frequency (RF) measurement community. This calibration technique requires well defined standards and establishes the reference planes of the corrected measurements near the tips of the probes used to measure the devices. Several other "probe-tip" calibration techniques are also widely used for on-wafer measurements, including line-reflect-match (LRM) [6] and line-reflect-reflect-match (LRRM) [7], [8]. The thru-reflect-line (TRL) calibration [9] is another staple of on-wafer microwave measurements. This method uses the redundancy of measurement results to define the reflection coefficient and propagation constant of the line standard [10]. The major draw back of the original TRL calibration technique, however, is that it is inherently frequency limited. Additional line standards were included to overcome this limitation with the aid of statistical analyses of the redundant measurement data. Several approaches were developed to this end including a weighted least squares method [11], a generalized distance regression method [12], and an orthogonal distance regression method [13]. The multiline TRL (mTRL) algorithm developed at the National Institute of Standards and Technology [13], [14] is considered the de facto standard technique for precision on-wafer calibration and measurements [10].

A considerable amount of work has been devoted to comparing and analyzing the different on-wafer calibration techniques. In the seminal work of Williams et al. [15], several on-wafer calibration techniques were compared using a new verification technique for determining the measurement accuracy of calibrated S-Parameters. A comparison of the accuracy and repeatability of on-wafer calibration techniques up to 110 GHz was reported in [16]. In [17], an excellent summary of the pitfalls in on-wafer calibration at mm-wave frequencies is presented. Probst et al. reported a comparison of 110 GHz on-wafer measurements in [18]. A comparison of on-wafer TRL and SOLT calibrations for measurements up to 500 GHz was reported by Fregonese et al. in [19]. The conclusions of many of these works are that the mTRL calibration algorithm is superior for on-wafer measurements at mm-wave frequencies.

There is considerably less work in the literature which compares and analyzes the effects of calibration on large-signal measurements. In [20], a procedure and metrics for comparing large-signal network analyzer (LSNA) calibrations were reported. An LSNA round robin exercise was reported by Barmuta et al. in [21]. A robust approach for the comparison and validation of large-signal measurement systems was also reported in [22]. None of these works explore the effect of different calibration techniques on on-wafer load-pull measurements of unmatched transistors.

In this work, a thorough empirical analysis of calibration effects on W-band scalar load-pull measurements is presented. First, in Section II, a comparison of S-Parameter measurements calibrated with the LRRM and on-wafer mTRL methods is presented. These comparisons are similar to what was reported in the literature regarding on-wafer calibrations for small-signal measurements. However, the aim of this section is to analyze aspects of the S-parameter measurements which are germane to load-pull measurements. Section III presents a novel investigation of calibration effects on the large-signal measurements of on-wafer unmatched GaN HEMTs. Different waveguide probes are used to highlight the effects of using the LRRM calibration algorithm and a similar investigation is conducted using the on-wafer mTRL calibration. Section IV concludes the article.

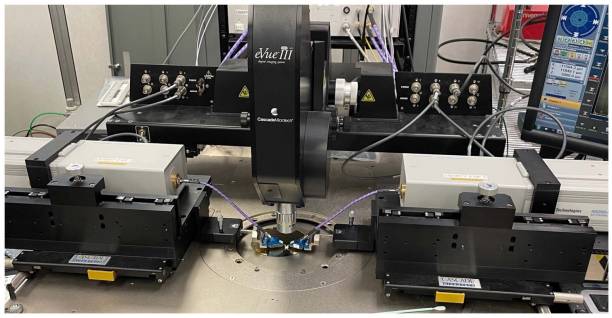

FIGURE 1. The 10 MHz–110 GHz on-wafer S-Parameter measurement system used to characterize the mm-wave GaN transistors.

II. SMALL-SIGNAL MEASUREMENTS

S-Parameter measurements were collected at the Air Force Research Laboratory (AFRL) Sensors Directorate using a 10 MHz–110 GHz continuous band on-wafer small-signal measurement bench illustrated in Fig. 1. The system is comprised of a Cascade 12 K probe station, an Agilent E8361 C 67 GHz PNA, an Agilent N5260 A mm-wave head controller, two OML N5260-60003 67–110 GHz frequency extenders, two Agilent N5260-60013 combiner assemblies which enable continuous band measurements across the full 10 MHz–110 GHz frequency range, and an Agilent E5270 A source/measure unit (SMU). Supply voltages were applied to the transistors through external bias tees which reside in the Agilent combiner assemblies. Three different 1 mm coaxial ground-signal-ground (GSG) RF probes were used to measure the S-parameters of the GaN HEMTs across a broad frequency range of 500 MHz to 110 GHz. The probes were FormFactor ACP 100 μm GSG, FormFactor infinity 100 μm GSG, and GGB picoprobe 100 μm GSG, which will be referred to as ACP, i110, and GGB throughout this work, respectively.

The on-wafer S-Parameter measurement system was first calibrated with the three separate pairs of coaxial probes using the LRRM calibration algorithm. The system configured with the FormFactor ACP and i110 probes was calibrated using a FormFactor 104-783 A impedance standard substrate (ISS). The system configured with the GGB probes was calibrated using the GGB CS-5 ISS. All calibrations were accomplished using the FormFactor WinCal software and with the proper inputs associated with each pair of probes. Custom settings were used for the GGB probes and calibration substrate. An absorber was placed under each ISS for calibration.

After calibration, a delay line was measured on the ISS to ensure that the calibrated S-Parameter measurements passed qualitative inspection and did not exhibit any irregularities.

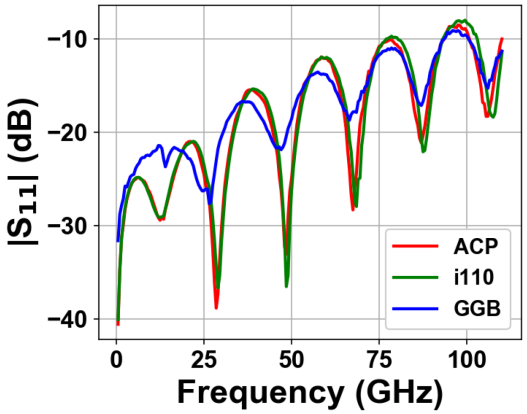

FIGURE 2. Measured S_{11} of a FormFactor ISS delay line with each pair of coaxial probes.

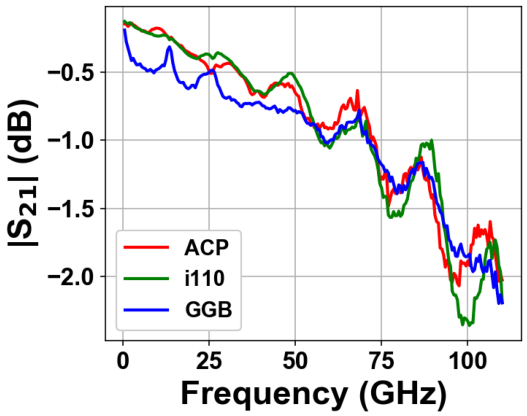

FIGURE 3. Measured S_{21} of a FormFactor ISS delay line with each pair of coaxial probes.

Figs. 2 and 3 report the calibrated S-Parameter measurements of a FormFactor delay line using each pair of coaxial probes. These results indicate each calibration provides similar results with the different pairs of probes and using the LRRM calibration algorithm. The minor difference in the calibrated measurement collected with the GGB probes highlights the issue of using calibration standards on a different substrate than the substrate of the DUT. The GGB probes were calibrated using the GGB ISS, and the delay line was measured on the FormFactor ISS.

A mm-wave GaN HEMT in a coplanar waveguide (CPW) configuration was measured using the LRRM calibrated S-Parameter test bench. The transistor was biased at $V_{DS} = 10$ V and $I_D = 100$ mA/mm. Fig. 4 reports the measured input small-signal reflection coefficient, S_{11}, of the GaN HEMT collected with the three different sets of RF probes. The measurements collected with the ACP, i110, and GGB probes are illustrated with solid red, green, and blue lines, respectively. Good agreement between the three sets of measurements is observed up to ∼13 GHz. However, the measurements above this particular frequency do not exhibit good agreement and considerable discrepancies are observed. The input small-signal conjugate match (SSCM), S_{11}^*, computed at 94 GHz

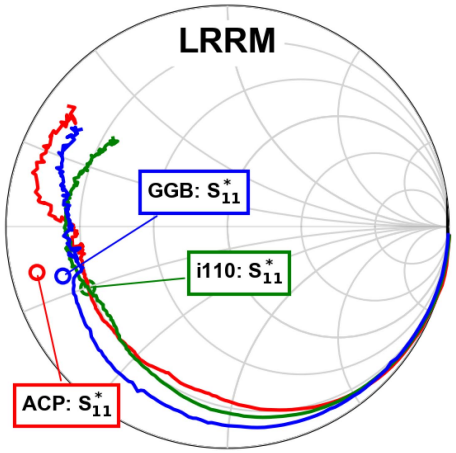

FIGURE 4. Measured input reflection coefficient, S_{11}, of a CPW GaN HEMT at a single bias using three different coaxial RF probes calibrated with the LRRM algorithm. The measurements exhibit good agreement up to ∼13 GHz. The input small-signal conjugate matches, S_{11}^*, computed from the three measurements at 94 GHz are illustrated with circles.

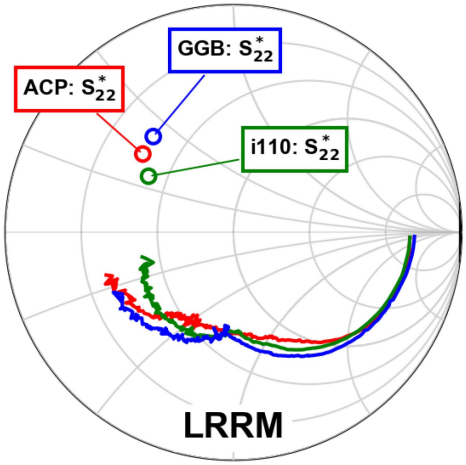

FIGURE 5. Measured output reflection coefficient, S_{22}, of a CPW GaN HEMT at a single bias using three different coaxial RF probes calibrated with the LRRM algorithm. The measurements exhibit good agreement up to ∼13 GHz. The input small-signal conjugate matches, S_{22}^*, computed from the three measurements at 94 GHz are illustrated with circles.

is also illustrated in Fig. 4. It is evident that the SSCM of the GaN HEMT is different when measured with the three separate sets of RF probes. This poses a considerable challenge in the context of on-wafer scalar load-pull measurements. RF transistors are typically impedance matched at the input using the SSCM, and therefore the transistor may not be optimally matched when measuring with different sets of probes due to limitations of the passive impedance tuners [4].

The measured output small-signal reflection coefficient, S_{22}, of the CPW GaN HEMT collected with the three RF probes is reported in Fig. 5. The output reflection coefficients diverge at a particular frequency of ∼13 GHz. The output SSCM, S_{22}^*, is plotted for the measurements collected with the different RF probes. The same transistor measured at an identical quiescent bias exhibits different output SSCMs when

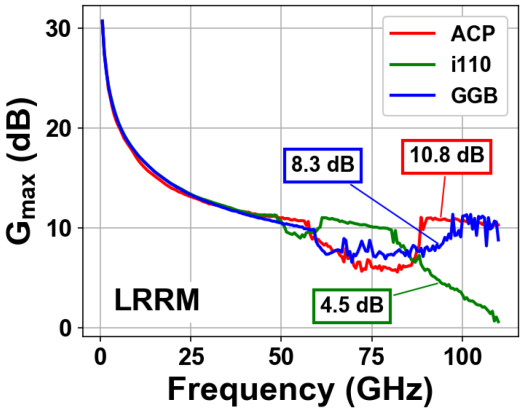

FIGURE 6. Maximum small-signal gain of a CPW GaN HEMT at a single bias using three different coaxial RF probes calibrated with the LRRM algorithm. The measurements exhibit good agreement up to ∼40 GHz. Values of maximum gain are reported at 94 GHz.

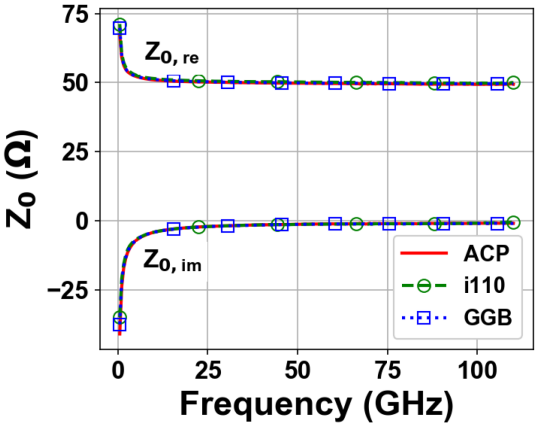

FIGURE 7. Calculated characteristic impedance, Z_0, of the on-wafer CPW transmission line using the mTRL algorithm with each pair of coaxial probes.

TABLE 1. Summary of LRRM Calibrated Small-Signal Measurement Absolute Differences

Probes	$\max\{\lvert\Delta S_{11}\rvert\}$	$\max\{\lvert\Delta S_{22}\rvert\}$	$\max\{\lvert\Delta G_{max}\rvert\}$
ACP − i110	0.26	0.23	9.7 dB
ACP − GGB	0.21	0.16	3.3 dB
i110 − GGB	0.20	0.22	10.0 dB

collected with different sets of RF probes calibrated with the LRRM algorithm. RF transistors rarely exhibit optimal large-signal metrics including output power and power added efficiency (PAE) at their output SSCM. However, this initial analysis sheds light on the potential differences in optimal transistor load impedances that could be collected with mm-wave on-wafer load-pull measurement systems.

Fig. 6 presents the maximum small-signal gain, G_{max}, of the CPW GaN HEMT calculated from S-Parameter measurements collected with the three sets of RF probes. It is interesting that good agreement between G_{max} collected with the different probes is observed up to ∼40 GHz. However, above this particular frequency, the measured values exhibit drastic differences. This is especially evident in the W-band frequency range. To highlight this, Fig. 6 also illustrates the computed values of G_{max} at 94 GHz. The maximum small-signal gain values of the same transistor are 4.5 dB, 8.2 dB, and 10.8 dB when measured with the i110, GGB, and ACP probes, respectively. This is a vast difference in the maximum small-signal gain of the same transistor collected with different RF probes. These results have a direct impact on large-signal measurements collected on the mm-wave transistors. A higher measured gain implies a potentially higher calculated PAE. A summary of the absolute differences between the S-Parameter measurements collected with each pair of coaxial probes and calibrated with the LRRM algorithm is reported in Table 1.

Next, on-wafer S-Parameter measurements of a mm-wave GaN HEMT in a CPW extended reference plane (ERP) configuration are investigated. The "intrinsic" component of this on-wafer unmatched transistor is nominally the same as the CPW transistor measured with LRRM calibration. However, the ERP transistor included CPW traces which connect the GSG pads and the intrinsic component of the transistor. The mTRL algorithm was used for calibrating the S-Parameter measurement system configured with the three sets of different RF probes. Well-designed on-wafer calibration structures were used for the mTRL calibrations. The on-wafer calibration kit included a thru, two shorts for each port, and three delay lines with lengths 200 μm, 400 μm, and 1400 μm. The same sets of ACP, i110, and GGB probes and the same on-wafer calibration kit were used for measuring the S-Parameters of the ERP transistor. The calibrations were verified by analyzing the resulting transmission line characteristic impedances determined by the mTRL algorithm. Fig. 7 illustrates the CPW transmission line characteristic impedance determined with the mTRL algorithm and with the three separate pairs of coaxial probes. These results indicate a consistent calibration.

The measured input small-signal reflection coefficient of the ERP transistor collected with the three pairs of RF probes and using the mTRL calibration is reported in Fig. 8. The measurements collected with the ACP, i110, and GGB probes are plotted with red, green, and blue lines, respectively. All three measurements exhibit excellent agreement up to 100 GHz, with a small shift observed in the measurements collected with the i110 probes above 100 GHz. The input SSCM computed at 94 GHz is included in Fig. 8. It is clear that the measurements collected using the three different sets of RF probes are very consistent when the system is calibrated using the on-wafer mTRL algorithm and well-designed calibration standards.

Fig. 9 illustrates the measured output small-signal reflection coefficients collected with the three different sets of RF probes and using the mTRL calibration algorithm. Good agreement between all three measurements is observed across the entire

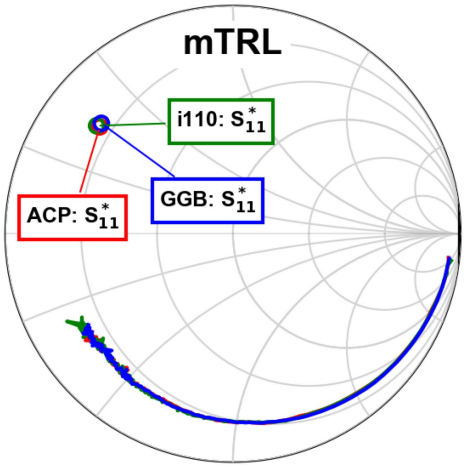

FIGURE 8. Measured input reflection coefficient, S_{11}, of an ERP GaN HEMT at a single bias using three different coaxial RF probes calibrated with the mTRL algorithm. The measurements exhibit excellent agreement across the entire frequency range. The input small-signal conjugate matches, S_{11}^*, computed from the three measurements at 94 GHz are illustrated with circles.

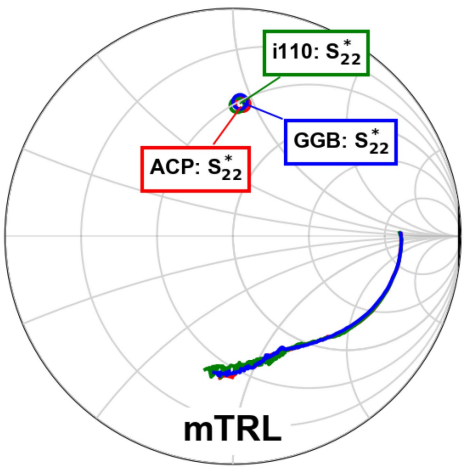

FIGURE 9. Measured output reflection coefficient, S_{22}, of an ERP GaN HEMT at a single bias using three different coaxial RF probes calibrated with the mTRL algorithm. The measurements exhibit excellent agreement across the entire frequency range. The input small-signal conjugate matches, S_{22}^*, computed from the three measurements at 94 GHz are illustrated with circles.

frequency range. Minor discrepancies are observed in the measurements above 50 GHz which could be due to small variations in probe placements on the calibration structures and on the measured ERP transistor. These measured results also provide good evidence that the on-wafer mTRL calibration provides consistent measurements regardless of the choice of RF probes.

Finally, the maximum small-signal gain of the ERP transistor computed from the S-Parameter measurements collected with the three sets of RF probes and calibrated with the mTRL algorithm is presented in Fig. 10. The values of G_{max} at 94 GHz are 8.67 dB, 8.78 dB, and 8.79 dB when the same transistor is measured using the GGB, i110, and ACP

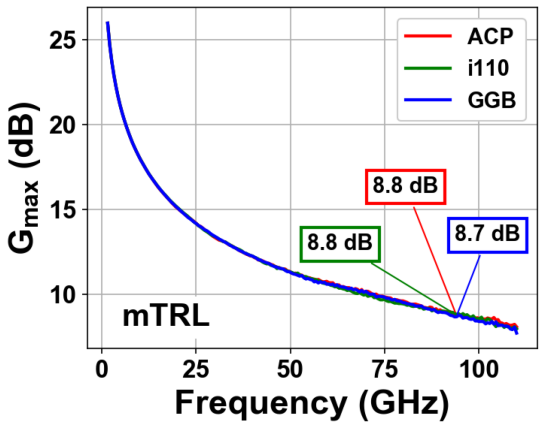

FIGURE 10. Maximum small-signal gain of an ERP GaN HEMT at a single bias using three different coaxial RF probes calibrated with the mTRL algorithm. The measurements exhibit excellent agreement across the entire frequency range. Values of maximum gain are presented at 94 GHz.

TABLE 2. Summary of mTRL Calibrated Small-Signal Measurement Absolute Differences

Probes	$\max\{\lvert\Delta S_{11}\rvert\}$	$\max\{\lvert\Delta S_{22}\rvert\}$	$\max\{\lvert\Delta G_{max}\rvert\}$
ACP − i110	0.09	0.10	0.4 dB
ACP − GGB	0.05	0.04	0.4 dB
i110 − GGB	0.10	0.06	0.3 dB

probes, respectively. These results provide further evidence that the mTRL calibration algorithm with well-designed calibration structures exhibits very consistent measurements up to 110 GHz. A summary of the absolute differences between the mTRL calibrated S-Parameter measurements collected with each pair of coaxial probes is reported in Table 2.

III. LARGE-SIGNAL MEASUREMENTS

The large-signal response of the mm-wave GaN HEMTs is next investigated using different combinations of waveguide probes and calibration algorithms. The on-wafer W-band scalar load-pull measurement system at AFRL was used to characterize the mm-wave GaN HEMTs [4]. This measurement system is a good candidate to conduct this analysis as it has been used extensively to characterize mm-wave GaN HEMT technologies [23], [24]. A picture of the W-band on-wafer scalar load-pull system is presented in Fig. 11. The components of the measurement system include a Keysight N5183B 40 GHz signal generator, a MI-WAVE 936W-85/105/20/387 WR-10 6x frequency multiplier, a MI-WAVE 511 W/387ND WR-10 programmable attenuator, a QuinStar QBP-94024030-H002 93–95 GHz 10 W solid state power amplifier, two Keysight E8486A-201 WR-12 extended frequency and dynamic range power sensors, two Flann 27333-3E W-band switches, two Virginia Diodes, Inc. WR-10 frequency extenders, two Maury MT979AL WR-10 automated mechanical impedance tuners, an Agilent E5273 A SMU, and a

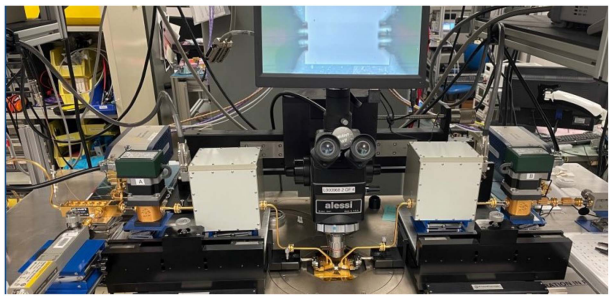

FIGURE 11. W-band (75 GHz–110 GHz) on-wafer scalar load-pull measurement system used to characterize the mm-wave GaN transistors.

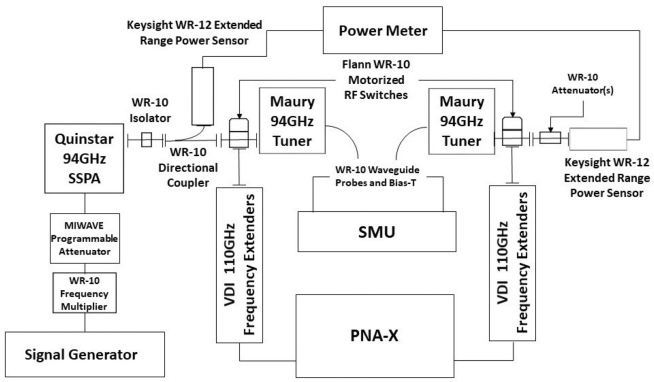

FIGURE 12. Block diagram of the W-band on-wafer scalar load-pull measurement system.

Keysight N5273B PNA-X. A block diagram of the W-band scalar load-pull system is illustrated in Fig. 12.

First, measurements of the on-wafer unmatched GaN HEMT in CPW configuration were investigated. Two sets of WR-10 waveguide probes were used to characterize the transistor. Namely, a pair of FormFactor ACP WR-10 100 μm probes and a pair of GGB picoprobe WR-10 100 μm probes were used. The LRRM calibration algorithm was used for both S-Parameter measurements on this system and also for the in-situ tuner characterization process required for scalar load-pull measurements. The FormFactor 104–783 A ISS was used for calibrating the system with the ACP WR-10 probes and the GGB CS-5 ISS was used for calibrating the system with the GGB WR-10 probes. An absorber was placed under both the FormFactor ISS and the GGB ISS. Again, all calibrations were accomplished using the FormFactor WinCal software.

The impedances of the passive W-band source and load tuners were set using the following procedure. First, the input and output SSCMs of the transistors were calculated from the S-Parameter measurements collected on the W-band load-pull system in its S-Parameter measurement configuration. Then, the impedances of the passive tuners were set as close to the calculated SSCMs as possible. The prescription of impedances based on the SSCMs enables a simplified analysis of the transistor power measurements without the need

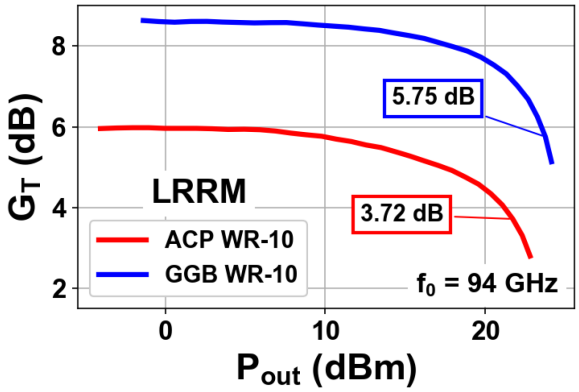

FIGURE 13. Measured transducer gain versus output power of the CPW GaN HEMT at 94 GHz fundamental frequency using the ACP WR-10 and GGB WR-10 probes. The LRRM algorithm was used to calibrate the system for these measurements.

for high power load-pull which could degrade the transistor performance.

The measured transducer gain, G_T, versus output power is reported in Fig. 13. Here, the red line represents the measurements collected with the ACP WR-10 probes and the blue line represents the measurements collected with the GGB WR-10 probes. The power sweeps were collected at a 94 GHz fundamental frequency with the transistor biased at $V_{DS} = 10$ V and $I_D = 100$ mA/mm. The ΔG_T metrics of the measurements collected with the ACP WR-10 and the GGB WR-10 probes were 0.17 dB and −0.06 dB, respectively. These verification metrics provide confidence in the precision of the on-wafer load-pull measurements. There is a substantial difference in the measured transducer gain collected with the load-pull system configured with the ACP WR-10 and GGB WR-10 probes. A difference of over 2 dB in G_T is observed in both the small-signal and large-signal regimes of Fig. 13. The large-signal gain highlighted in Fig. 13 was analyzed at the input power corresponding to peak PAE. The discrepancies in the measurements of the exact same transistor at nominally the same operating conditions (i.e., quiescent bias, frequency, matching conditions) appear to be due to using the LRRM calibration with different waveguide probes.

Fig. 14 reports the PAE of the CPW transistor collected with both sets of waveguide probes calibrated with the LRRM algorithm. Again, the red line represents the measurements collected with the ACP WR-10 probes and the blue line represents measurements collected with the GGB WR-10 probes. It is clear that the PAE of the transistor is substantially affected by the choice of waveguide probes. In this example, the PAE varies by nearly 24 percentage points – a 125% increase. This amount of variation in PAE of on-wafer unmatched transistors is due to utilizing different waveguide probes with the LRRM calibration algorithm. This can cause considerable disagreements when benchmarking mm-wave transistor technologies at independent RF measurement laboratories.

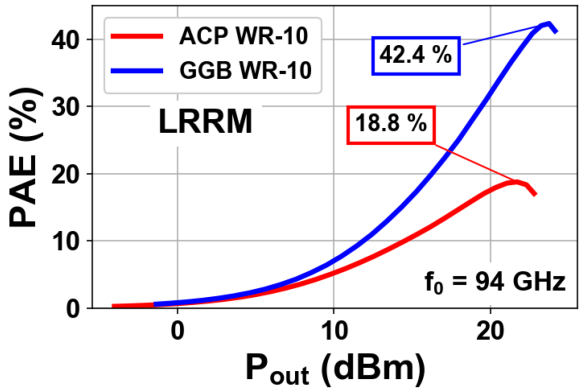

FIGURE 14. Transistor PAE versus output power of the CPW GaN HEMT at 94 GHz fundamental frequency using the ACP WR-10 and GGB WR-10 probes. The LRRM algorithm was used to calibrate the system for these measurements.

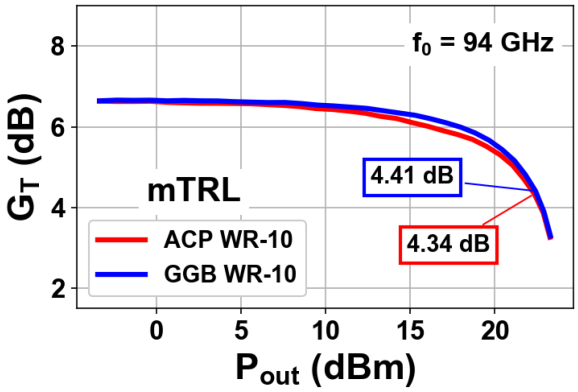

FIGURE 15. Measured transducer gain versus output power of the ERP GaN HEMT at 94 GHz fundamental frequency using the ACP WR-10 and GGB WR-10 probes. The mTRL algorithm was used to calibrate the system for these measurements.

TABLE 3. Summary of LRRM Calibrated Large-Signal Measurements. The Output Power and Gain Were Evaluated At the Input Power Corresponding to Peak PAE

Probes	Absorber	ΔG_T (dB)	Peak PAE (%)	P_{out} (W/mm)	G_T (dB)
ACP WR-10	Yes	0.17	18.8	1.48	3.72
GGB WR-10	No	-0.20	28.2	1.93	4.85
GGB WR-10	Yes	-0.06	42.4	2.37	5.75

The on-wafer unmatched transistor was load pulled to investigate whether the large variation in PAE could be overcome by choice of a load impedance other than the SSCM. However, the transistor moderately responded to a high power load pull and did not exhibit an increase in PAE on the same order as what was observed with a different pair of probes. Therefore, the substantial variation in large-signal measurements is attributed to the LRRM calibration algorithm.

As a final example, the on-wafer W-band scalar load-pull system was re-characterized with the GGB WR-10 probes, the LRRM calibration, and without the absorber under the GGB CS-5 ISS. The on-wafer CPW transistor was re-measured using identical operating conditions as the previous two measurement sets. The results are added to the summary of LRRM calibrated data in Table 3. Clearly, the off-wafer LRRM calibration algorithm is highly sensitive to the choice of W-band waveguide probes and whether an absorber was placed under the ISS. This sensitivity yields drastically different large-signal measurements of the same on-wafer unmatched GaN HEMT when collected with different probes.

Next, the on-wafer ERP GaN HEMT was measured with the same W-band scalar load-pull system and pairs of waveguide probes. The load-pull system was characterized using the on-wafer mTRL calibration algorithm and the on-wafer calibration standards associated with the ERP transistor. Special care was taken to ensure consistent probing of the calibration standards and transistor using the two sets of waveguide probes. The source and load impedances presented to the transistors were set as close to the measured SSCM as possible within the limits of the passive measurement system. The measured SSCM collected with the two pairs of waveguide probes were similar to the results presented in Figs. 8 and 9.

Fig. 15 illustrates the measured transducer gain versus output power of the ERP transistor at 94 GHz fundamental frequency and $V_{DS} = 10$ V and $I_D = 100$ mA/mm quiescent bias. The measurements collected with the ACP WR-10 and GGB WR-10 probes are plotted with red and blue lines, respectively. The calculated ΔG_T metrics of the large-signal measurements collected with the ACP WR-10 and the GGB WR-10 probes were -0.15 dB and -0.35 dB, respectively. Again, this provides confidence in the on-wafer load-pull system calibration and the conclusions drawn from the measurements collected with this system. Both sets of power sweep measurements exhibit excellent agreement despite the fact that separate waveguide probes were used to collect the measurements. The difference in the measured large-signal transducer gain is <0.1 dB. This is in stark contrast to the measurements collected using the same waveguide probes on a similar on-wafer unmatched transistor but using the LRRM calibration algorithm.

The PAE of the ERP transistor collected using both sets of waveguide probes and the on-wafer mTRL calibration algorithm is presented in Fig. 16. Again, the measurements collected with the ACP WR-10 and the GGB WR-10 probes are illustrated with red and blue lines, respectively. These results indicate that the measurements collected with two substantially different waveguide probes exhibit excellent agreement with each other. Specifically, the difference in the peak PAE collected with both pairs of waveguide probes is <1 percentage point. This result provides confidence that measurements collected using a system calibrated with the on-wafer mTRL calibration algorithm and well-design calibration structures are not affected by choice of waveguide

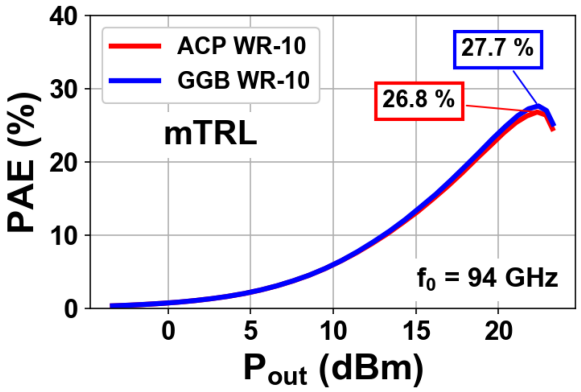

FIGURE 16. Transistor PAE versus output power of the ERP GaN HEMT at 94 GHz fundamental frequency using the ACP WR-10 and GGB WR-10 probes. The mTRL algorithm was used to calibrate the system for these measurements.

TABLE 4. Summary of mTRL Calibrated Large-Signal Measurements. The Output Power and Gain Were Evaluated At Peak PAE

Probes	ΔG_T (dB)	Peak PAE (%)	P_{out} (W/mm)	G_T (dB)
ACP WR-10	-0.15	26.8	1.71	4.34
GGB WR-10	-0.35	27.7	1.74	4.41

probe. A summary of the mTRL calibrated large-signal measurements is provided in Table 4.

IV. CONCLUSION

This article presented a thorough analysis of the effects of calibration on small-signal and large-signal on-wafer measurements of unmatched mm-wave GaN HEMTs. Specifically, this work detailed a comparison of LRRM calibrated on-wafer S-Parameters measurements collected with three different types of coaxial RF probes and on-wafer load-pull measurements collected with two types of waveguide probes. It was found that the LRRM calibrated S-Parameter measurements of a single CPW GaN HEMT exhibited substantial variations in the calculated SSCM and in the maximum small-signal gain. A variation of over 6 dB in maximum small-signal gain was observed in the LRRM calibrated measurements with different RF probes. Furthermore, the LRRM calibrated on-wafer load-pull measurements of a single CPW GaN HEMT exhibited a large variation in measured gain and PAE. The measured large-signal transducer gain varied by over 2 dB and the peak PAE varied by over 24 percentage points. mTRL calibrated on-wafer S-Parameter measurements of a single ERP GaN HEMT exhibited minimal variation when collected with three different coaxial RF probes. Variations in the maximum small-signal gain were less than 0.1 dB. The mTRL calibrated on-wafer load-pull measurements of a single ERP GaN HEMT also demonstrated excellent precision when collected with two sets of waveguide probes. The measured large-signal gain varied by less than 0.1 dB and the peak PAE varied by less than 1 percentage point. These results provide quantitative evidence that the on-wafer mTRL calibration algorithm combined with well-designed on-wafer calibration structures are the preferred choice for precision on-wafer large-signal measurements at mm-wave frequencies. If it is not possible to calibrate the on-wafer load-pull system using on-wafer mTRL with quality calibration structures, then it is preferred to use consistent probes, calibration algorithm, and ISS when comparing measurements of different mm-wave on-wafer unmatched transistor technologies.

REFERENCES

[1] M. Guidry et al., "W-band passive load pull system for on-wafer characterization of high power density N-polar GaN devices based on output match and drive power requirements vs. gate width," in *Proc. IEEE 87th ARFTG Microw. Meas. Conf.*, 2016, pp. 1–4.

[2] V. Teppati et al., "A *W*-band on-wafer active load-pull system based on down-conversion techniques," *IEEE Trans. Microw. Theory Techn.*, vol. 62, no. 1, pp. 148–153, Jan. 2014.

[3] J. Zhang, J. Urbonas, G. Esposito, A. Arias-Purdue, and P. Rowell, "On-wafer, large-signal transistor characterization from 70–110 GHz using an optimized load-pull technique," *Microw. J.*, vol. 64, no. 2, pp. 82–90, 2021.

[4] N. C. Miller, M. Elliott, R. Gilbert, E. Arkun, and D. J. Denninghoff, "Surmounting W-band scalar load-pull limitations using the ASM-HEMT model for millimeter-wave GaN HEMT technology large-signal assessment," in *Proc. 99th ARFTG Microw. Meas. Conf.*, Denver, CO, USA, 2022, pp. 1–4. [Online]. Available: https://ieeexplore.ieee.org/document/9896585/

[5] A. Rumiantsev, *On-Wafer Calibration Techniques Enabling Accurate Characterization of High-Performance Silicon Devices at the mm-Wave Range and Beyond*. Gistrup, Denmark: River Publishers, 2019.

[6] H.-J. Eul and B. Schiek, "Thru-match-reflect: One result of a rigorous theory for de-embedding and network analyzer calibration," in *Proc. IEEE 18th Eur. Microw. Conf.*, 1988, pp. 909–914.

[7] A. Davidson, K. Jones, and E. Strid, "LRM and LRRM calibrations with automatic determination of load inductance," in *IEEE 36th ARFTG Conf. Dig.*, 1990, pp. 57–63.

[8] L. Hayden, "An enhanced line-reflect-reflect-match calibration," in *Proc. IEEE 67th ARFTG Conf.*, San Francisco, CA, USA, 2006, pp. 143–149. [Online]. Available: https://ieeexplore.ieee.org/document/4734364/

[9] G. Engen and C. Hoer, "Thru-reflect-line: An improved technique for calibrating the dual six-port automatic network analyzer," *IEEE Trans. Microw. Theory Techn.*, vol. 27, no. 12, pp. 987–993, Dec. 1979.

[10] A. Rumiantsev and N. Ridler, "VNA calibration," *IEEE Microw. Mag.*, vol. 9, no. 3, pp. 86–99, Jun. 2008. [Online]. Available: https://ieeexplore.ieee.org/document/4519498/

[11] D. Blackham, "Application of weighted least squares to OSL vector error correction," in *IEEE 61st ARFTG Conf. Dig.*, 2003, pp. 11–21.

[12] M. Salter, N. Ridler, and P. Harris, "Over-determined calibration schemes for RF network analysers employing generalised distance regression," in *Proc. IEEE 62nd Conf. ARFTG Microw. Meas.*, 2003, pp. 127–142.

[13] D. Williams, J. Wang, and U. Arz, "An optimal vector-network-analyzer calibration algorithm," *IEEE Trans. Microw. Theory Techn.*, vol. 51, no. 12, pp. 2391–2401, Dec. 2003.

[14] R. Marks, "A multiline method of network analyzer calibration," *IEEE Trans. Microw. Theory Techn.*, vol. 39, no. 7, pp. 1205–1215, Jul. 1991. [Online]. Available: https://ieeexplore.ieee.org/document/85388/

[15] D. F. Williams, R. B. Marks, and A. Davidson, "Comparison of on-wafer calibrations," in *IEEE 38th ARFTG Conf. Dig.*, San Diego, CA, USA, 1991, pp. 68–81. [Online]. Available: https://ieeexplore.ieee.org/document/4119616/

[16] A. J. Lord, "Comparing the accuracy and repeatability of on-wafer calibration techniques to 110GHz," in *Proc. IEEE 29th Eur. Microw. Conf.*, 1999, pp. 28–31.

[17] V. Krozer et al., "On-wafer small-signal and large-signal measurements up to sub-THz frequencies," in *Proc. IEEE Bipolar/BiCMOS Circuits Technol. Meeting*, 2014, pp. 163–170.
[18] T. Probst, R. Doerner, M. Ohlrogge, R. Lozar, and U. Arz, "110 GHz on-wafer measurement comparison on alumina substrate," in *Proc. IEEE 90th ARFTG Microw. Meas. Symp.*, 2017, pp. 1–4.
[19] S. Fregonese et al., "Comparison of on-wafer TRL calibration to ISS solt calibration with open-short de-embedding up to 500 GHz," *IEEE Trans. THz Sci. Technol.*, vol. 9, no. 1, pp. 89–97, Jan. 2019.
[20] D. F. Williams, K. A. Remley, J. M. Gering, G. S. Lyons, C. Lineberry, and G. S. Aivazian, "Comparison of large-signal-network-analyzer calibrations," *IEEE Microw. Wireless Compon. Lett.*, vol. 20, no. 2, pp. 118–120, Feb. 2010.
[21] P. Barmuta et al., "Comparing LSNA calibrations: Large-signal network analyzer round robin," *IEEE Microw. Mag.*, vol. 17, no. 2, pp. 59–64, Feb. 2016.
[22] T. Williams et al., "A robust approach for comparison and validation of large signal measurement systems," in *IEEE MTT-S Int. Microw. Symp. Dig.*, 2008, pp. 257–260.
[23] J.-S. Moon et al., "W-band graded-channel GaN HEMTs with record 45% power-added-efficiency at 94 GHz," *IEEE Microw. Wireless Compon. Lett.*, vol. 33, no. 2, pp. 161–164, Feb. 2023. [Online]. Available: https://ieeexplore.ieee.org/document/9907865/
[24] A. Arias-Purdue et al., "N-polar GaN HEMTs in a high-uniformity 100-mm wafer process with 43.6 and 2 W/mm at 94 GHz," *IEEE Microw. Wireless Technol. Lett.*, early access, Apr. 10, 2023, doi: 10.1109/LMWT.2023.3263058.

NICHOLAS C. MILLER (Senior Member, IEEE) received the B.S., M.S., and Ph.D. degrees in electrical and computer engineering from Michigan State University, in 2013, 2015, and 2017, respectively. He is an Electronics Engineer with Air Force Research Laboratory Sensors Directorate, Dayton, OH, USA. He is currently a young professional member of the IEEE MTT-3 Microwave Measurements Committee. His technical interests span a broad range of fundamental, applied, and computational physics, applied mathematics, electrical engineering, linear and nonlinear RF characterization, and linear and nonlinear RF modeling and simulation. Dr. Miller was the recipient of IEEE AP-S PreDoctoral research award in 2013, a U.S. DoD science, mathematics, and research for transformation scholarship in 2014, IEEE Dayton Section Harrell V. Nobel award in 2019 for physics-based device modeling, the best conference paper award at the 21st IEEE wireless and microwave technology conference (WAMICON) in 2021, and the best presentation award at the IEEE MTT-S Young Professional Workshop on Optimization and Modeling of Active Devices in 2022.

MICHAEL ELLIOTT is currently working toward the undergraduate degree in electrical engineering with Arizona State University, Tempe, AZ, USA. He started as a contractor in 2006 working on site with AFRL. For the last 10 years, he has been in the electrical field and also on site. He is currently an RF Test Technician. His work specializes in passive and active load pull, noise parameter measurements, millimeter wave measurements, as well as large and small signal device characterizations.

EYTHAN LAM (Member, IEEE) received the B.S degree in electrical engineering from the University of California, Santa Barbara, Santa Barbara, CA, USA, in 2020. He is currently working toward the Ph.D. degree with UCSB. His research interests include high-efficiency power amplifier design in upper millimeter wave bands and predistortion.

RYAN GILBERT (Member, IEEE) received the Bachelor of Science in electronics engineering technology from DeVry University, Naperville, IL, USA. Since 2010, has been a contractor and working on site with AFRL. He is currently a Senior RF Test Engineer, specializing in active and passive load pull, millimeter wave measurements, vector signal analysis, as well as small and large signal characterization. Before joining AFRL, his background included designing and constructing RF resonators for MRI research.

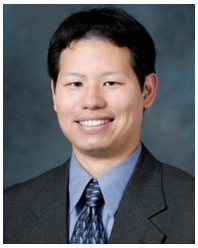

JANSEN UYEDA received the B.S. degree in electrical engineering from the University of Hawaii, Honolulu, HI, USA and the M.S. degree in electrical engineering from the University of Southern California, Los Angeles, CA, USA. He was a member of technical staff in 1997, Northrop Grumman Space Systems (previously T.R.W. Space & Electronics), Redondo Beach, CA, USA, where he was responsible for lithography operations in the GaAs HBT and HEMT production line. He is currently a Sr. Staff Engineer supporting development and maturation of GaN technologies.

ROBERT L. COFFIE (Senior Member, IEEE) received the B.S. degree in engineering physics from the University of Oklahoma, Norman, OK, USA in 1997 and the Ph.D. degree in electrical and computer engineering from the University of California, Santa Barbara, Santa Barbara, CA, USA, in 2003. He is a Senior Staff Engineer in Microelectronic Semiconductors with Northrop Grumman. He has designed, developed, and matured AlGaN/GaN HEMT technologies for RF applications from L-band to Q-band with Northrop Grumman and TriQuint Semiconductor (now Qorvo). He also developed the first JEDEC qualified AlGaN/GaN HEMTs for 600 V power switching applications with Transphorm, where he was the Director of device engineering. He holds 13 patents and has authored or coauthired more than 30 journal articles related to AlGaN/GaN HEMTs, a book chapter on new materials for high power RF applications, and the book *2D Electrostatics* (2021 CRC Press).